Noncovalent Functionalization of Boron Nitride Nanotubes with Poly(*p*-phenylene-ethynylene)s and Polythiophene

Singaravelu Velayudham,[†] Chee Huei Lee,[‡] Ming Xie,[‡] Dominique Blair,[†] Nicholas Bauman,[†] Yoke Khin Yap,*,[‡] Sarah. A. Green,[†] and Haiying Liu*,[†]

Department of Chemistry and Department of Physics, Michigan Technological University, 1400 Townsend Drive, Houghton, Michigan

ABSTRACT Boron nitride nanotubes (BNNTs) are functionalized and solubilized in organic solvents such as chloroform, methylene chloride, and tetrahydrofuran by using conjugated poly(*p*-phenylene ethynylene)s (PPEs) (polymers **A** and **B**) and polythiophene (polymer **C**) via a noncovalent functionalization approach through strong $\pi-\pi$ stacking interactions between the conjugated polymers and BNNTs. The functionalization of BNNTs with PPEs enhanced planarization of PPEs with red shifts in both absorbance and emission of the composite materials with reference to free PPEs, whereas the functionalization of BNNTs with polythiophene disrupts the π-conjugation, resulting in blue shifts in both the absorption and emission of the composite material.

KEYWORDS: noncovalent functionalization • boron nitride nanotubes • poly(*p*-phenylene-ethynylene) • polythiophene • fluorescence

INTRODUCTION

Boron nitride nanotubes (BNNTs) are wide band gap semiconductors regardless of the tube diameter, chirality, or number of walls. As a result, they are different from carbon nanotubes (CNTs), which can be either semimetallic (1) or semiconducting (2). BNNTs are electrically insulating and thermally conducting materials. BNNTs can be produced by laser ablation (3−5), arc discharge (66, 7), chemical vapor deposition (8−10), thermal annealing (11), substitution reaction (12), and solid-state processing (13). Direct growth of high-purity BNNTs on substrate has also been demonstrated using plasma-enhanced pulsed laser deposition (PLD) (14) at a temperature as low as 600 °C. Except for the PLD approach, most of these techniques produce BNNTs with significant impurities and require further functionalization and purification processes prior to applications. Because BNNTs possess excellent mechanical (15, 16), electronic (17, 18), and thermal (19, 20) properties, functionalization of BNNTs will facilitate BNNT applications in high mechanical strength fibers, electrical insulator, and thermal conducting materials for chemical, mechanical stability, and resistance to oxidation at higher temperature.

Nanotubes such as CNTs and BNNTs are not soluble in any common solvents as they have a tendency to aggregate. Noncovalent and covalent functionalization approaches have been used to functionalize and solubilize CNTs. Noncovalent functionalization approaches have advantages over covalent functionalization approaches since they can keep intrinsic properties of CNTs such as high mechanical strengths and conductivity without disruption of extended π-conjugation systems of CNTs. Noncovalent and covalent functionalization approaches for CNTs have been extended to functionalize and solubilize BNNTs. However, it limits to a few cases. BNNTs have been functionalized and solubilized in chloroform by using poly[m-phenylenevinylene-co-(2,5-dioctoxyp-phenylenevinylene)] (21) for purification of BNNTs via the wrapping approach with $\pi-\pi$ stacking interactions between the polymer and BNNTs (22). Covalent linking of diamine terminated polyethylene glycol (PEG) (23) to the surface of BNNTs has been demonstrated and used to tune the band gap of BNNTs (24). Self-organized composite films of BNNTs and polyaniline were prepared by sonicating the mixture of BNNTs and polyaniline in N,N-dimethylformamide through efficient $\pi-\pi$ interaction between the polyaniline and the BNNTs (25). In this article, we extend our unique noncovalent functionalization approach of CNTs to functionalize the BNNTs by using poly(p-phenylene-ethynylene)s and compare this approach with one by using polythiophene. We demonstrated that BNNTs have effectively been functionalized and solubilized by using conjugated poly(p-phenylene-ethynylene)s (polymers **A** and **B**) and polythiophenes (polymer **C**) (Scheme 1). The composite materials are expected to have a potential application in high mechanical strength fibers (26).

Scheme 1. Chemical Structures of PPEs (Polymers A and B) and Regioregular Head-to-Tail Polythiophene (Polymer C)
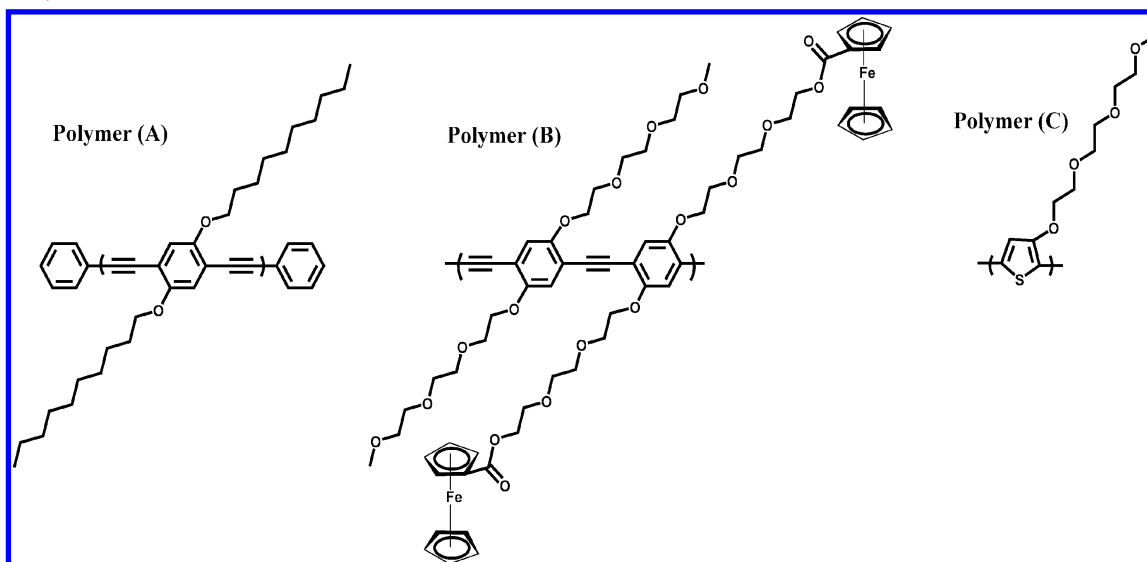
EXPERIMENTAL DETAILS

BNNTs grown by thermal chemical vapor deposition (Thermal CVD) were used in our experiments for surface functionalization (27). In brief, B, MgO, and FeO (with 2:1:1 molar ratio) were mixed by a mortar and pestle. These powders are transferred to an alumina combustion boat and loaded into a closed-end test tube. Subsequently, this setup is placed into a horizontal tube furnace. NH_3 with a flow rate of 200 mL/h is then introduced to the quartz chamber after evacuation to ~4 Pa. After 1 h of growth at 1200 °C, a white product was uniformly deposited over the side wall of the combustion boat. As-grown BNNTs were characterized using Hitachi S-4700 field emission scanning electron microscope under operating voltage at 5 kV and with working distance 12 mm, and Tecnai F20ST (S) transmission electron microscope with operating voltage at 200 kV.

Composite materials of BNNTs with each conjugated polymer were prepared by adding 2 mg of BNNTs to a solution containing 2 mg of the conjugated polymer in 6 mL of chloroform. The suspension was sonicated for 15 min. The resulting solution was then centrifuged at 2000 rpm for 10 min to remove any nonsoluble impurities. Ten μL of composite solution of polymer **A** and BNNTs was deposited onto a silicon substrate and then held vertically to align the nanotubes. The excess solvent flowed down was absorbed by a Kimwipe. The composite membrane was spin coated on silicon substrate at 2000 rpm by using of 50 μL of composite solution of polymer A and BNNTs.

UV−visible absorption spectra were recorded using a Perkin-Elmer Lambda 35 instrument. The composite spectra were background corrected against BNNTs dispersed in $CHCl_3$ solvent to enhance the signal. The fluorescence spectra of the composite materials were recorded using a Fluoromax spectrofluorometer with an excitation wavelength of 410 nm for polymers **A** and **B** and their composite materials, and 375 nm for polymer **C** and its composite material. The slit width was set to 5 nm and all the samples were scanned with an increment of 1 nm.

Fluorescence lifetime was determined by using the stroboscopic technique on a PTI instrument equipped with a pulsed N_2 laser, pumping dye lasers [Bis-MSB; $\lambda_{absorption} = 421$ nm in p-dioxane and PBD; $\lambda_{absorption} = 366$ nm in toluene/ethanol (50:50)] with excitation wavelengths of 410 and 380 nm. Data were deconvoluted with PTI software using a 2-exponential fit. Fluorescence quantum yields were calculated by taking fluorescein as standard with 85 % relative to quantum yield in 0.1 M NaOH (28, 29).

^{1}H NMR spectra were obtained by using 400 MHz Varian Unity Inova spectrophotometer instrument. $CDCl_3$ was used and the chemical shifts (δ) were given in ppm relative to the solvent peak of 7.24 ppm as an internal standard. The schematic representations of molecular models were obtained by using HyperChem 7.5 software. Molecular weights of the polymers were determined by gel permeation chromatography (GPC) by using a Waters Associates Model 6000A liquid chromatograph. Mobile phase was HPLC grade THF which were filtered and degassed by vacuum filtration through a 0.5 μm Fluoropore filter prior to use. The polymers were detected by a Waters Model 440 ultraviolet absorbance detector at a wavelength of 254 nm and a Waters Model 2410 refractive index detector. Molecular weight was measured relative to polystyrene standards.

Poly(p-phenylene-ethynylene)s [polymer **A** (30) and polymer **B** (31)] were prepared and characterized according to reported procedures. Gel permeation chromatography analysis (mobile phase: THF, polystyrene standards) indicates that M_n of polymers **A** and **B** are 22 300 and 28 000 g/mol and their polydispersities are 2.2 and 1.9, respectively. Regioregular head-to-tail polythiophene (polymer **C**) was prepared and characterized according to a reported procedure (32−34). Gel permeation chromatography analysis (mobile phase: THF, polystyrene standards) indicates that M_n of polymer **C** is 16 500 g/mol and its polydispersity is 1.6.

RESULTS AND DISCUSSION

Scanning electron microscopy (SEM) and high resolution transmission electron microscopy were used to characterize as-grown BNNTs and their composite materials. The as-grown BNNTs possess very high crystallinity and well-defined tubular structures (Figure 1a,b). The side-walls of these BNNTs are very clean with no detectable amorphous coatings.

BNNTs were functionalized and solubilized by mixing BNNTs with poly(p-pheneylene-ethynylene) (PPE, polymer A) in chloroform, sonicated and purified by centrifuge. There is not significant color change of PPE compared with its composite material. One mg of BNNTs can be dissolved in 3 mL of choroform in the presence of PPE, and the resulting composite solution is transparent (Figure 2). Polymer **A** displays an absorption maximum at 444 nm (Figure 3b),
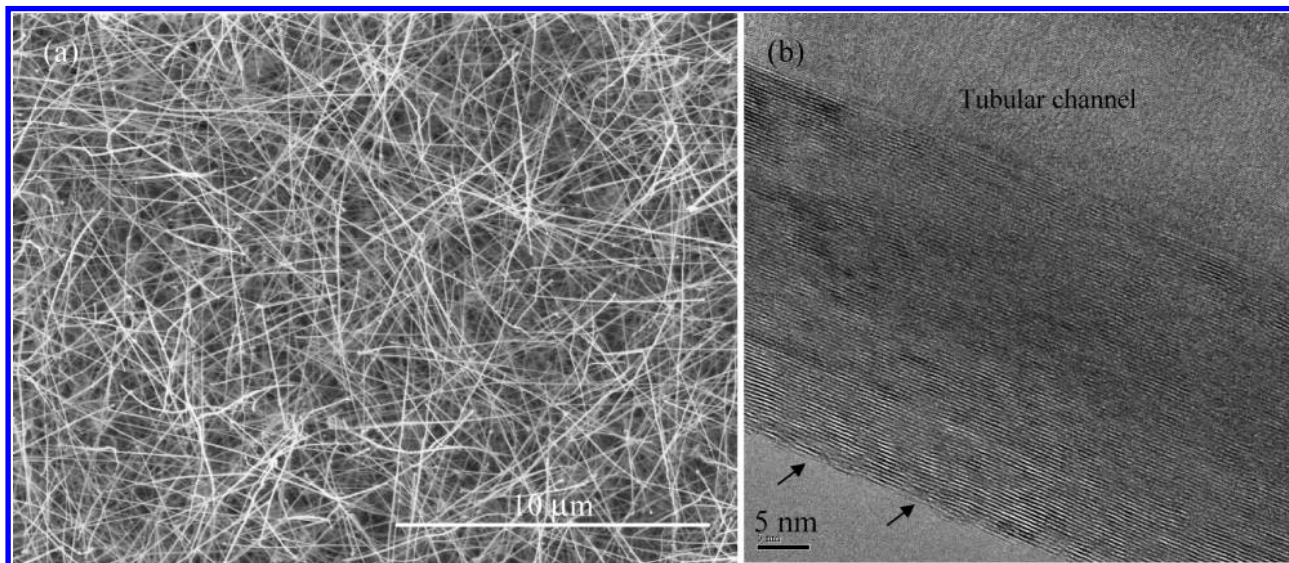
FIGURE 1. (a) SEM image of as-grown BNNTs dispersed in ethanol spin coated on silica substrate. (b) High-resolution TEM image of BNNT side walls (arrows) without amorphous coatings.

FIGURE 2. Digital photo picture of composite solution of BNNTs and polymer A in CHCl₃.

FIGURE 3. (a) Fluorescence spectra of polymer A (dark line) and composite of BNNTs and polymer A in CHCl₃ (dash line), (b) absorption spectrum of polymer A (dark line), and corrected absorption spectrum of composite of BNNTs and polymer A (dash line) in CHCl₃

corresponding to the $\pi-\pi^*$ absorption of poly(p-pheneylene-ethynylene) backbone. It exhibits an emission maximum at 474 nm, which corresponds to the relaxation transition from the lowest excited singlet state energy level to the ground state. Composite material of polymer **A** and BNNTs (composite **A**) in CHCl₃ shows an emission maximum at 503 nm with a significant red shift of 29 nm relative to an emission maximum of polymer **A** (Figure 3a). Composite **A** in CHCl₃ solution also displays a red shift with a maximum absorbance at 499 nm (Figure 3b). BNNTs show no significant absorption band in the region 300 to 700 nm because their absorption band falls in the UV region with a band gap ~5.9 eV (27). The red shifts in both absorption and emission of composite material of BNNTs and polymer **A** are attributed to the enhanced π-conjugation of the polymer in its composite material through $\pi-\pi$ stacking interactions between PPEs and BNNTs (35, 36). The similar red shifts in both absorption and emission of PPEs were also reported in composite materials of PPEs and CNTs because of strong $\pi-\pi$ stacking interactions between PPEs and CNTs (30, 37).

¹H NMR spectra of polymer A in its composite material in CDCl₃ showed that the peak at 6.99 ppm corresponding to protons of phenyl groups become smaller compared with that of free polymer, indicating $\pi-\pi$ stacking interactions
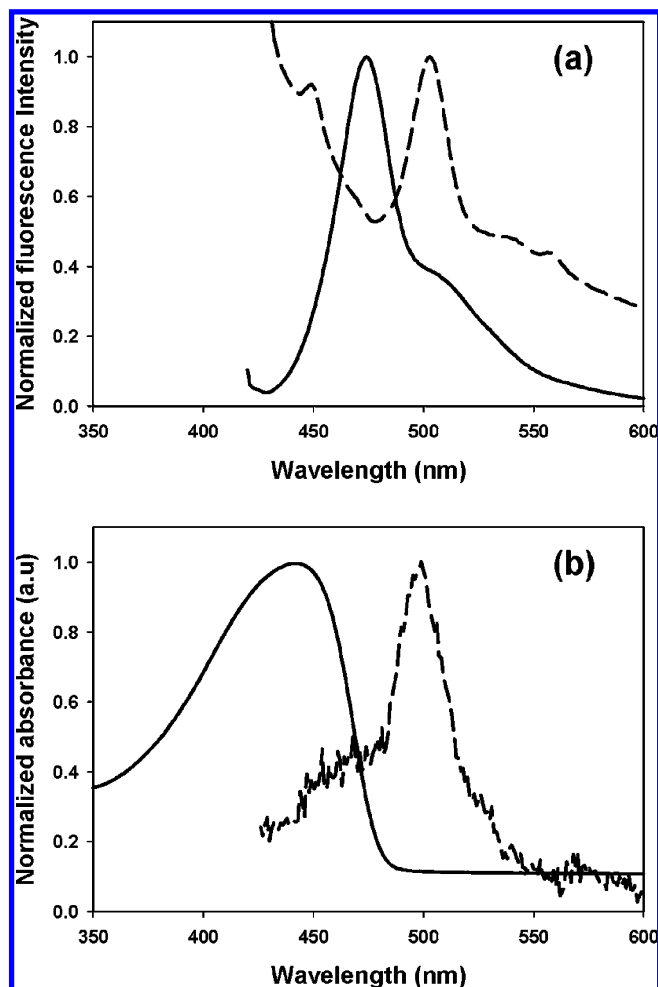
between PPEs and BNNTs. The alkyl protons of polymer side chains become a little broader after functionalization of BNNTs with polymer **A** (see Figures S1 and S2 in the
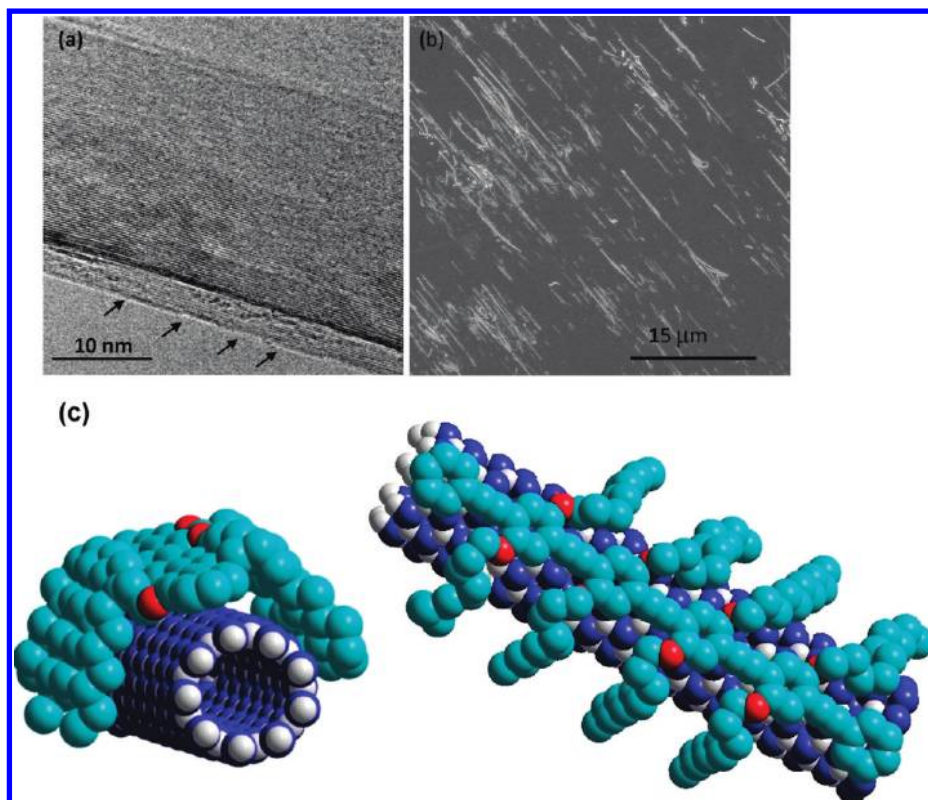
FIGURE 4. (a) High-resolution TEM image at the BNNT side walls functionalized with PPE (polymer A). A layer of PPE can be clearly seen as indicated by arrows. (b) SEM image of aligned BNNTs functionalized with polymer A. (c) Schematic models of composite material of BNNTs and polymer A at various viewing angles.

Supporting Information). High-resolution TEM imaging of BNNT functionalized with polymer **A** shows a layer of polymer **A** with less than 1 nm in thickness at the side-walls (Figure 4a). These functionalized BNNTs have well-ordered tubular structures with wall thicknesses of ∼30 nm, indicating that BNNTs still retain the crystalline morphology after functionalization. The similar results were also observed in other composite materials of BNNTs with poly(p-phenylene-ethynylene) bearing ferrocence residues (polymer **B**) or regioregular head-to-tail polythiophene (polymer **C**). We further examine the dispersion of these BNNTs by coating the composite solution on a silicon substrate as alignment of CNTs has been prepared by using composite solution of PPEs and CNTs to demonstrate that the solubility of the composite materials (30). SEM image of composite materials of polymer A and BNNTs shows that BNNTs are well-dispersed and aligned along the flow direction of the solution (Figure 4b). Scanning electron microscope image of composite membrane of BNNTs and polymer A on silicon substrate showed that BNNT surfaces were coated with PPEs (see Figure S3 in the Supporting Information). The molecular model of composite material of BNNTs and polymer **A** obtained by using Hyperchem software shows that PPE backbone attaches to the BNNT surface through $\pi-\pi$ stacking interactions (Figure 4c), which helps enhance π-conjugated of PPE while the polymer side chains are flexible, which enhances solvation of BNNTs and solubilizes BNNTs in the organic solvent.

It is reported that poly(p-phenylene-ethynylene) bearing ferrocene residues (polymer **B**) has significantly enhanced solubility of CNTs compared with poly(p-phenylene-ethynylene) bearing decyl side chains (polymer **A**) as ferrocene groups also involve $\pi-\pi$ interactions with CNTs (30). We would like to test whether poly(p-phenylene-ethynylene) bearing ferrocene residues with alkyl tethered spacers (polymer **B**) can enhance the solubility of BNNTs. Polymer **B** in chloroform solution shows the absorbance maximum at 432 nm and the emission maximum at 471 nm (Figure 5). Composite of polymer **B** and BNNTs in chloroform also displays significant red shifts of 68 and 33 nm in both absorption and emission because of the enhanced π-conjugation of PPEs in the composite materials compared with polymer **B** (Figure 5). However, PPE bearing ferrocene residues did not enhance solubility of BNNTs in chloroform compared with polymer **A (**Table 1).

Poly[m-phenylenevinylene-co-(2,5-dioctoxyp-phenylenevinylene)] as a wrapping conjugated polymer has been used to functionalize and solubilize CNTs and BNNTs in chloroform through $\pi-\pi$ stacking interactions between the polymer and CNTs (38) or BNNTs (21). Poly[m-phenylenevinylene-co-(2,5-dioctoxyp-phenylenevinylene)] in the composite materials show significant blue shifts in absorption and emission compared with its pure polymer because the wrapping of the polymer around CNTs or BNNTs disrupt π-conjugation of the polymer backbone. Our noncovalent functionalization approach of BNNT with PPEs results in significant red shift in both absorption and emission of PPEs because of the enhanced coplanarity of PPE π-conjugation via strong $\pi-\pi$ strong interactions between PPEs and BNNTs. Schematic model of composite of polymer **A** and
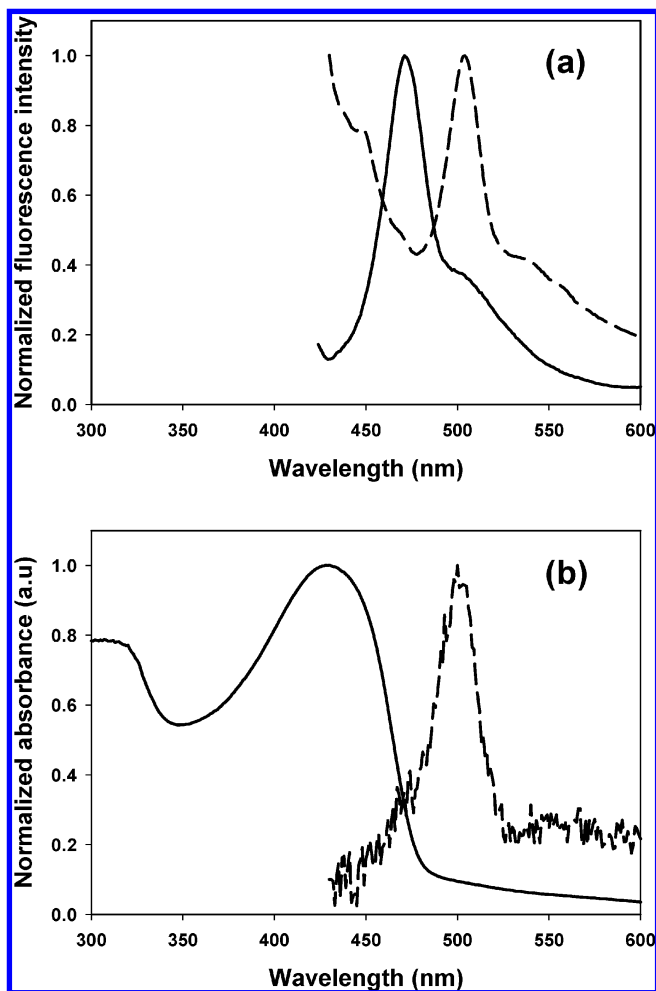
FIGURE 5. (a) Fluorescence spectra of polymer B (dark line) and its composite material with BNNTs (dashed line) in CHCl₃, (b) absorption spectrum of polymer B (dark line), corrected spectrum of composite material of BNNTs and polymer B (dash line) in CHCl₃.

Table 1. Solubility of BNNTs in the Presence of Polymer A, B, or C in CHCl₃

polymer	solubility of BNNT (mg/mL)
polymer A	~0.30
polymer B	~0.30
polymer C	~0.22

BNNTs shows polymer backbone stacked onto the nanotube surface of BNNTs, resulting in enhanced coplanarity of PPE in the composite materials (Figure 4c). For comparison, we chose a regioregular head-to-tail polythiophene bearing tri-(ethylene glycol) methyl ether side chains (polymer C) to functionalize and solubilize BNNTs as a potential wrapping polymer because this polymer backbone can be twisted as poly[m-phenylenevinylene-co-(2,5-dioctoxyp-phenylenevinylene]. The composite material of polymer C and BNNTs displays significant blue shift of 50 and 42 nm in both absorption and in emission as the composite material shows an absorbance maximum at 330 nm and an emission maximum at 433 nm, respectively (Figure 6). The blue shifts of polymer **C** in the composite material indicate that π-conjugation of the polythiophene is disrupted and that the polythiophene wraps around BNNTs through $\pi-\pi$ stacking
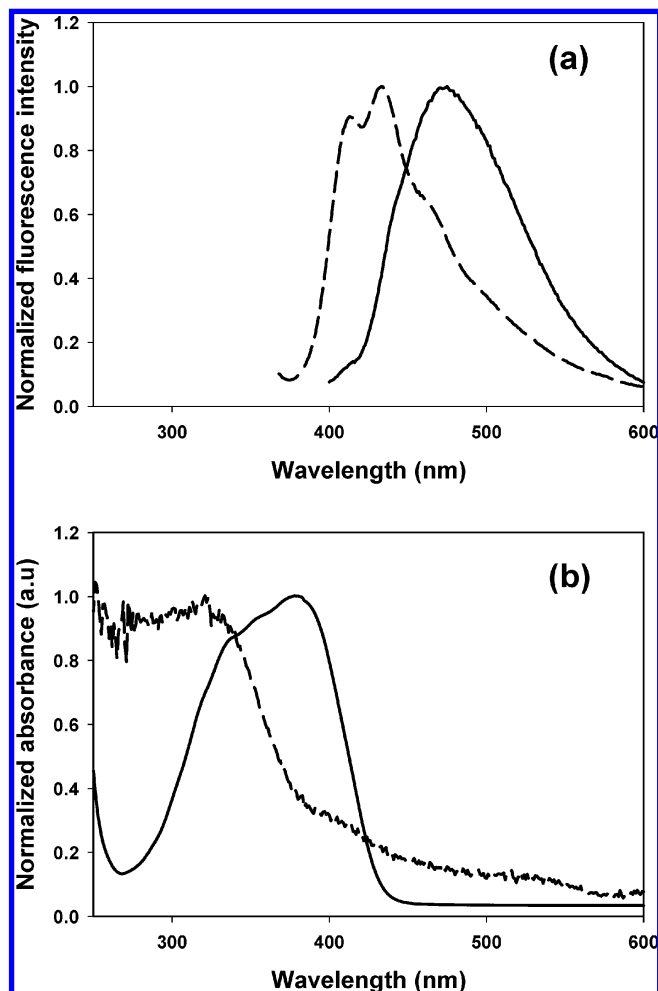

FIGURE 6. (a) Fluorescence emission spectra of polymer C (dark line) and its composite with BNNTs (dashed line) in CHCl₃. (b) Absorption spectrum of polymer C (dark line), corrected spectrum of composite material of BNNTs and polymer C (dash line) in CHCl₃.

interactions between polythiophene and BNNTs. The functionalization of BNNTs with polymer **B** or polymer **C** also resulted in no distinct color change as it was observed in the case of polymer **A**.

The functionalization of CNTs with PPEs resulted in complete quenching of the polymer fluorescence (30). In contrast, the functionalization of BNNTs is expected not to result in complete fluorescence quenching as BNNTs are insulators. In order to further probe the effect of noncovalent functionalization of BNNTs on the fluorescence of the polymers, we characterized photophysical properties of the polymers and their composite materials such as absorption maxima, emission maxima, quantum yield, Stokes shift, and excited state lifetime determinations (Table 2). The quantum yields and excited state lifetimes of polymers **A** and **B** in their composite materials are greater than their pure polymers, which is presumably due to enhanced planarization of the backbone induced by $\pi-\pi$ stacking interactions of PPEs and BNNTs. However, the quantum yield and excited state lifetime of polythiophene in its composite material is slightly smaller than its pure polymer, suggesting that the helix shape of polythiophene wraps around the BNNT and enhances a nonradiative decay path. The increased fluores-

Table 2. Optical Properties of Polymers A, B, C, and Their Composite Materials in CHCl₃

	polymer **A**	composite **A**	polymer **B**	composite **B**	polymer **C**	composite **C**
$\lambda_{abs.max}$ (nm)	444	499	432	500	380	330
$\lambda_{emis.max}$ (nm)	474	503	471	504	475	433
Stoke shift (nm)	30	4	39	4	95	103
quantum yield (%)	15	37	9	21	4	3
lifetime (ns)	0.44	1.20 (0.95)	0.27 (0.69)	0.58 (0.85)	0.18 (0.87)	0.11 (0.73)
		0.49 (0.05)	0.10 (0.31)	0.24 (0.15)	0.08 (0.13)	0.16 (0.27)

cence lifetime in PPEs in composite materials could be due to enhanced exciton diffusion (39), and smaller values of Stoke shift results from the decreased vibrational motion because of the planarization of the backbone, which altogether decrease the probability of nonradiative decay paths.

The difference between the fluorescence maxima and the first band absorption maxima expressed in wave numbers, $\Delta\nu = \Delta\nu a - \Delta\nu f$, is known as Stokes shift. Lippert equation relates the polarity between solvent and the fluorophore, orientation, polarizability and the cavity area wherein the fluorophore resides to the Stokes shift (40). A higher value for Stokes shift and relationship of this value with increased in solvent polarity implies that the excited state dipole moment is greater than the ground state (40). The smaller Stokes shift of 4 nm observed in the case of PPE-based composite materials indicate that the dipole moment of the excited state of composites materials are similar to that of their ground state, presumably due to π-π stacking interactions between the polymer backbone and the nanotube wall surface. The smaller Stokes shift could also be a manifestation of fewer solvating molecules available for the polymer as they are now partially interacting with BNNTs through $\pi-\pi$ stacking interactions. The larger Stokes shift observed in the polythiophene (95 nm) and its composite material (103 nm) indicate that the relaxation from the excited state takes place through internal conversion at a higher rate competing the radiative decay rate from the highest excited state energy level. As a result, greater Stokes shift was observed for polythiophene and its composite materials.

Energy transfer mechanisms that take place within the polymers are complicated and extensive efforts have been made to relate that conformation, excited state dynamics, and energy transfer (39). In the case of nanocomposite materials of polymer and BNNTs, the conformation is different from that of the free polymer. This change in conformation resulted in red/blue shifts for the optical spectra. The enhanced quantum yield and lifetime indicate increased planarity on polymer chain in composite. As no charge-transfer band was observed in the absorption spectrum of composite materials, the emission is not a result of Forster energy transfer because of no overlap between the absorption spectrum of BNNT and emission spectrum of polymers.

The solutions of composite materials were stable for more than 6 months when they were stored in a refrigerator or at room temperature as long as the solutions were kept from evaporation. The complete solvent evaporation resulted in formation of the composite membranes during storage. However, the composite membranes can be dissolved in organic solvents after sonication.

The noncovalent functionalization of BNNTs with conjugated polymers can not only solubilize the BNNTs in common organic solvents but also provide an effective approach to tune the band gap of the resulting composite materials by choosing appropriate polymers. The composite materials of BNNTs and conjugated polymers have a potential application to prepare much higher mechanical strength fibers than composite materials of CNTs and conjugated polymers (30) as BNNTs possess much better mechanical strength than CNTs (16, 41).

CONCLUSION

A simple, effective noncovalent functionalization and solubilization of BNNTs has been achieved by using poly(p-phenylene-ethynylene)s and polythiophene through strong $\pi-\pi$ stacking interactions between conjugated polymers and BNNTs. The enhanced π-conjugation of PPEs in their composite materials is characterized by red shifts in absorption and fluorescence compared with those of the free polymers. High-resolution TEM and SEM confirm the morphology of BNNTs was not affected by the functionalization which can keep intrinsic properties of BNNTs for potential application to prepare high-mechanical-strength fibers. The fluorescence intensity of polymer was retained or enhanced after functionalization of BNNTs with conjugated polymers.

Supporting Information Available: NMR spectra of polymer and polymer/BNT composite and TEM images of BNT and polymer/BNT composite (PDF). This material is available free of charge via the Internet at http://pubs.acs.org.

REFERENCES AND NOTES
(1) Mintmire, J. W.; Dunlap, B. I.; White, C. T. *Phys. Rev. Lett.* **1992**, *68* (5), 631–634.
(2) Wilder, J. W. G.; Venema, L. C.; Rinzler, A. G.; Smalley, R. E.; Dekker, C. *Nature* **1998**, *391* (6662), 59–62.
(3) Yu, D. P.; Sun, X. S.; Lee, C. S.; Bello, I.; Lee, S. T.; Gu, H. D.; Leung, K. M.; Zhou, G. W.; Dong, Z. F.; Zhang, Z. *Appl. Phys. Lett.* **1998**, *72* (16), 1966–1968.
(4) Lee, R. S.; Gavillet, J.; de la Chapelle, M. L.; Loiseau, A.; Cochon,

J. L.; Pigache, D.; Thibault, J.; Willaime, F. *Phys. Rev. B: Condens. Matter Mater. Phys.* **2001**, *64* (12), 121405/121401−121404.

(5) Golberg, D.; Bando, Y.; Eremets, M.; Takemura, K.; Kurashima, K.; Yusa, H. *Appl. Phys. Lett.* **1996**, *69* (14), 2045−2047.

(6) Terrones, M.; Hsu, W. K.; Terrones, H.; Zhang, J. P.; Ramos, S.; Hare, J. P.; Castillo, R.; Prassides, K.; Cheetham, A. K.; Kroto, H. W.; Walton, D. R. M. *Chem. Phys. Lett.* **1996**, *259* (5−6), 568−573.

(7) Loiseau, A.; Willaime, F.; Demoncy, N.; Hug, G.; Pascard, H. *Phys. Rev. Lett.* **1996**, *76* (25), 4737−4740.

(8) Lourie, O. R.; Jones, C. R.; Bartlett, B. M.; Gibbons, P. C.; Ruoff, R. S.; Buhro, W. E. *Chem. Mater.* **2000**, *12* (7), 1808−1810.

(9) Zhi, C.; Bando, Y.; Tan, C.; Golberg, D. *Solid State Commun.* **2005**, *135* (1−2), 67−70.

(10) Ma, R.; Bando, Y.; Sato, T. *Chem. Phys. Lett.* **2001**, *337* (1−3), 61−64.

(11) Terauchi, M.; Tanaka, M.; Suzuki, K.; Ogino, A.; Kimura, K. *Chem. Phys. Lett.* **2000**, *324* (5−6), 359−364.

(12) Weiqiang, H.; Yoshio, B.; Keiji, K.; Tadao, S. *Appl. Phys. Lett.* **1998**, *73* (21), 3085−3087.

(13) Ying, C.; Lewis, T. C.; John Fitz, G.; James, S. W. *Appl. Phys. Lett.* **1999**, *74* (20), 2960−2962.

(14) Wang, J.; Kayastha, V. K.; Yap, Y. K.; Fan, Z.; Lu, J. G.; Pan, Z.; Ivanov, I. N.; Puretzky, A. A.; Geohegan, D. B. *Nano Lett.* **2005**, *5* (12), 2528−2532.

(15) Chopra, N. G.; Luyken, R. J.; Cherrey, K.; Crespi, V. H.; Cohen, M. L.; Louie, S. G.; Zettl, A. *Science* **1995**, *269* (5226), 966−967.

(16) Chopra, N. G.; Zettl, A. *Solid State Commun.* **1998**, *105* (5), 297−300.

(17) Radosavljevic, M.; Appenzeller, J.; Derycke, V.; Martel, R.; Avouris, P.; Loiseau, A.; Cochon, J.-L.; Pigache, D. *Appl. Phys. Lett.* **2003**, *82* (23), 4131−4133.

(18) Rubio, A.; Corkill, J. L.; Cohen, M. L. *Phys. Rev. B: Condens. Matter Mater. Phys.* **1994**, *49* (7), 5081−5084.

(19) Tang, C.; Bando, Y. *Appl. Phys. Lett.* **2003**, *83* (4), 659−661.

(20) Han, W.-Q.; Mickelson, W.; Cumings, J.; Zettl, A. *Appl. Phys. Lett.* **2002**, *81* (6), 1110−1112.

(21) Zhi, C.; Bando, Y.; Tang, C.; Xie, R.; Sekiguchi, T.; Golberg, D. *J. Am. Chem. Soc.* **2005**, *127* (46), 15996−15997.

(22) Zhi, C.; Bando, Y.; Tang, C.; Honda, S.; Sato, K.; Kuwahara, H.; Golberg, D. *J. Phys. Chem. B.* **2006**, *110* (4), 1525−152.

(23) Xie, S. Y.; Wang, W.; Fernando, K. A. S.; Wang, X.; Lin, Y.; Sun, Y. P. *Chem. Commun.* **2005**, (29), 3670−3672.

(24) Zhi, C. Y.; Bando, Y.; Tang, C. C.; Golberg, D. *Phys. Rev. B: Condens. Matter Mater. Phys.* **2006**, *74* (15), 153413−153414.

(25) Zhi, C. Y.; Bando, Y.; Tang, C. C.; Honda, S.; Sato, K.; Kuwahara, H.; Golberg, D. *Angew. Chem., Int. Ed.* **2005**, *44* (48), 7929−7932.

(26) Chen, J.; Ramasubramaniam, R.; Xue, C.; Liu, H. *Adv. Funct. Mater.* **2006**, *16* (1), 114−119.

(27) Chee Huei, L.; Jiesheng, W.; Vijaya, K. K.; Jian, Y. H.; Yoke Khin, Y. *Nanotechnology* **2008**, (19), 455605.

(28) Parker, C. A.; Rees, W. T. *Analyst* **1960**, *85*, 587−600.

(29) Crosby, G. A.; Demas, J. N. *J. Phys. Chem.* **1971**, *75* (8), 991−1024.

(30) Chen, J.; Liu, H.; Weimer, W. A.; Halls, M. D.; Waldeck, D. H.; Walker, G. C. *J. Am. Chem. Soc.* **2002**, *124* (31), 9034−9035.

(31) Xue, C.; Chen, Z.; Wen, Y.; Luo, F.-T.; Chen, J.; Liu, H. *Langmuir* **2005**, *21* (17), 7860−7865.

(32) Osaka, I.; McCullough, R. D. *Acc. Chem. Res.* **2008**, *41* (9), 1202−1214.

(33) Sheina, E. E.; Khersonsky, S. M.; Jones, E. G.; McCullough, R. D. *Chem. Mater.* **2005**, *17* (13), 3317−3319.

(34) Xue, C.; Luo, F.-T.; Liu, H. *Macromolecules* **2007**, *40* (19), 6863−6870.

(35) Bunz, U. H. F.; Imhof, J. M.; Bly, R. K.; Bangcuyo, C. G.; Rozanski, L.; Vanden Bout, D. A. *Macromolecules.* **2005**, *38* (14), 5892−5896.

(36) Miteva, T.; Palmer, L.; Kloppenburg, L.; Neher, D.; Bunz, U. H. F. *Macromolecules* **2000**, *33* (3), 652−654.

(37) Jian, C.; Cuihua, X.; Ramasubramaniam, R.; Haiying, L. *Carbon* **2006**, *44* (11), 2142−2146.

(38) Star, A.; Stoddart, J. F.; Steuerman, D.; Diehl, M.; Boukai, A.; Wong, E. W.; Yang, X.; Chung, S.-W.; Choi, H.; Heath, J. R. *Angew. Chem., Int. Ed.* **2001**, *40* (9), 1721−1725.

(39) Rose, A.; Tovar, J. D.; Yamaguchi, S.; Nesterov, E. E.; Zhu, Z.; Swager, T. M. *Philos. Trans. R. Soc., Ser. A* **2007**, *365* (1855), 1589−1606.

(40) Lakowicz, J. R. *Principles of Fluorescence Spectroscopy*, 3rd ed.; Springer: New York, 2006; pp 205−236.

(41) Golberg, D.; Costa, P. M. F. J.; Lourie, O.; Mitome, M.; Bai, X.; Kurashima, K.; Zhi, C.; Tang, C.; Bando, Y. *Nano Lett.* **2007**, *7* (7), 2146−2151.

AM900613J

Supporting Information

Non-covalent Functionalization of Boron Nitride Nanotubes with Poly(p-phenylene-ethynylene)s and Polythiophene

Singaravelu Velayudham,[1] Chee Huei Lee,[2] Ming Xie,[2] Dominique Blair,[1] Nicholas Bauman,[1] Yoke Khin Yap,[2,] Sarah. A. Green,[1] Haiying Liu,[1,**]*

[1]Department of Chemistry, Michigan Technological University, 1400 Townsend Drive, Houghton, MI, USA.

[2]Department of Physics, Michigan Technological University, 1400 Townsend Drive, Houghton, MI, USA.

AUTHOR EMAIL ADDRESSES: * ykyap@mtu.edu, ** hyliu@mtu.edu

The supporting information includes ^{1}H NMR spectra of polymer A and its composite material with BNNTs in $CDCl_3$, SEM image of as grown BNNTs dispersed in ethanol spin coated on silica substrate and SEM image of composite membrane of BNNTs and polymer **A** which was spin coated on silica substrate.
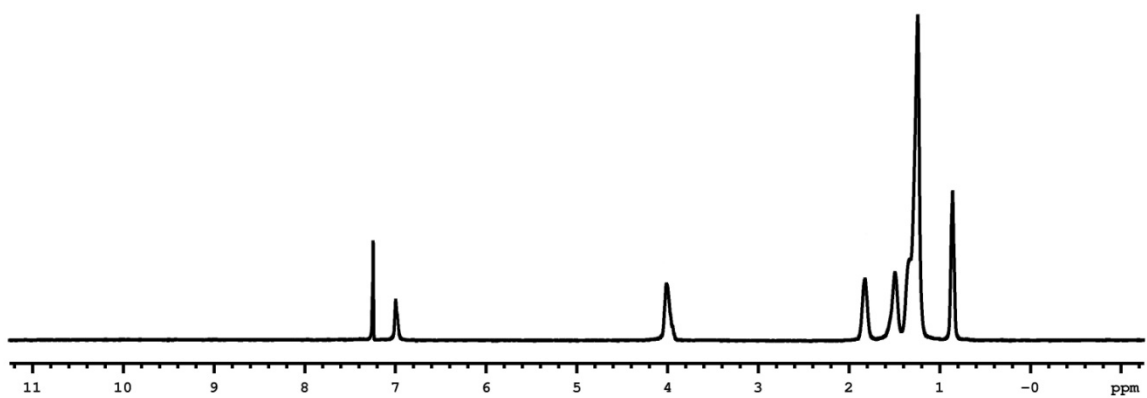
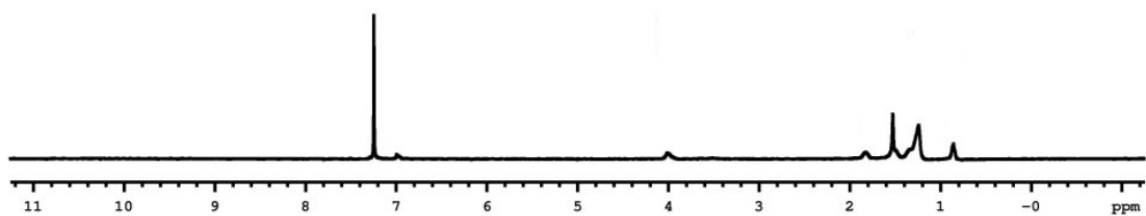**Figure S1.** ^{1}H NMR spectrum of polymer **A** in CDCl$_3$.

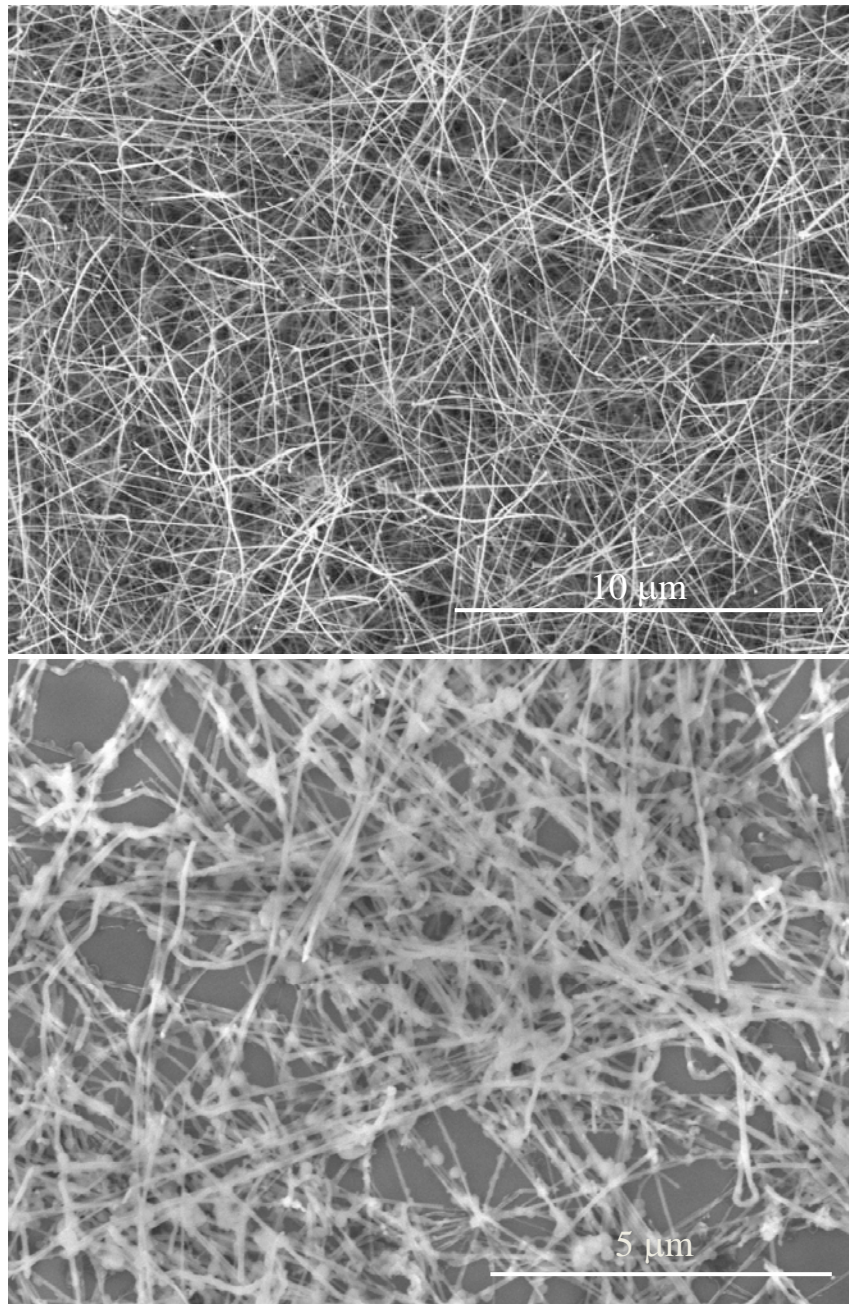**Figure S2.** ^{1}H NMR spectrum of composite material of BNNTs and polymer **A** in CDCl$_3$.

Figure S3. SEM image of as grown BNNTs dispersed in ethanol spin coated on silica substrate (upper picture), and SEM image of composite membrane of BNNTs and polymer **A** which was spin coated on silica substrate (lower picture).